Tunable Active Inductor Offers Integrable And Cost-Effective Alternatives of Varactor Tuned VCOs

[1,2]Ulrich L. Rohde, *Fellow, IEEE*
[1]Univ. of Cottbus, BTU Cottbus 03046, Germany
[2]Synergy Microwave Corporation, NJ 07504, USA

Ajay K. Poddar, *Senior Member, IEEE*
Synergy Microwave Corporation, NJ 07504, USA
akpoddar@synergymwave.com

***Abstract*—This paper describes the novel TAI (Tunable Active Inductor) configuration that enables reconfigurable voltage controlled oscillators (VCOs) for multi-band and multi-standard wireless applications. To demonstrate reconfigurality, reported TAI VCO simultaneously generates dual frequency bands using surface mounted device (SMD) components, and readily lends itself for fabrication in integrated-circuit form. The measured phase noise for band#1 (2450-2650 MHz) and band#2 (4850-5250 MHz) are typically better than -105 dBc/Hz at 100 kHz offset from the carrier with operating bias of 3V, 20mA.**

I. INTRODUCTION

One of the critical building blocks of a multi-mode trans-receiver system is a configurable multi-band voltage controlled oscillators (VCOs) that are required for both up and down conversion. Mobile phones and radios operating in several modes are typically switch between receiving frequencies and transmitting frequencies, and therefore, require reconfigurable oscillator in each of the switched bands.

A general problem in the VCO design is a trade-off between tuning range, phase noise and power consumption. The simplified approach for wideband VCO is a switched capacitor network for coarse tuning and a tuning varactor for fine-tuning, as shown in Figure (1). Such an arrangement can offer wideband tunability but at the cost of poor phase noise and power-consumptions.

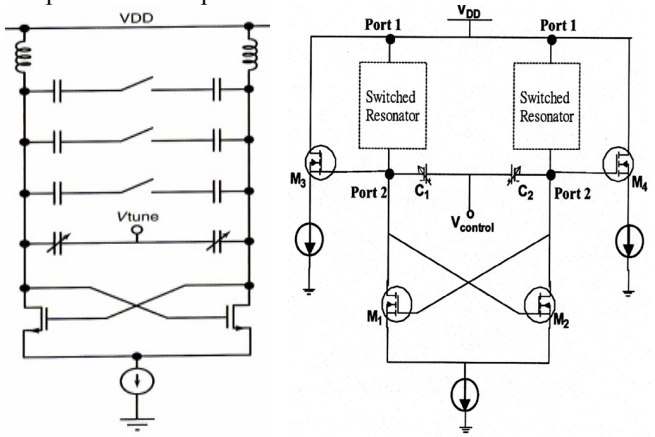

Fig.1. Multi-band VCO: (a) LC-VCO with switched capacitor network for coarse tuning and (b) dual-band VCO using switched resonator technology

Another option is set of parallel VCOs that can cover several frequency ranges. The advantage of this approach is now each VCO can be tailored for best phase noise, power consumption, and tuning range trade-off.

The main drawback of multiple VCOs solutions is a significantly increased die area, therefore, not a cost-effective alternative. To overcome the above problems, we propose a reconfigurable architecture using active tunable inductors (ATI) that synchronously generates multiple frequencies for different bands without using multiplier and switching, therefore, cost-effective and power-efficient solutions [1]-[15].

II. RECONFIGURABLE ARCHITECTURE

The coexistence of different wireless systems requires multi-band and multi-standard mobile terminals. Trans-receivers for multi-standard telephony are often implemented by replicating the receiver circuits for each operating band or standard. Multi-standard receivers typically use duplicate components, circuit blocks, or even entire radio receivers for each standard. Although, this approach is simpler to implement, but it is neither cost effective nor power efficient. Trans-receiver circuit in such a situation requires reconfigurable basic building elements (*R*, *L* and *C*) to share function between different standards in an adaptive manner.

A. Active Tunable Resistor (ATR)

Figure (2) shows the typical configuration of active resistor using 3-port transistor, where negative resistance is seen at any of the three ports if the remaining two of the ports are terminated with suitable impedances [4]. This allows negative input impedance if both Z_1 and Z_3 are of the same type (L or C). As shown in Figure (2), if Z_1 and Z_3 are capacitors, then base-emitter (bipolar) or gate-source (FETs) capacitances of the transistor can be embedded into Z_1 or else, when Z_1 and Z_3 are inductors, biasing RF choke can be part of the inductive Z_3.

The characteristics of capacitive feedback tunable resistor can be described by (Fig. 2)

$$R_{atr} = R = -\frac{Y_{21}(v_{be})}{\omega^2 C_{be} C_3} \Rightarrow R = -2\pi \frac{f_T}{\omega^2 C_3} \qquad (1)$$

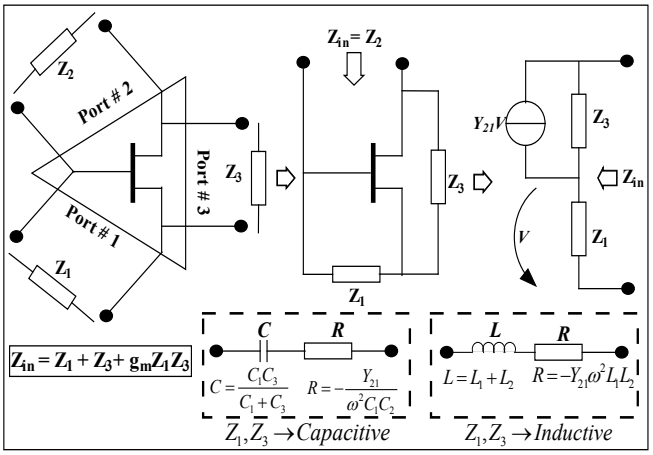

Fig.2. A typical schematic of negative tunable resistor using single transistor

Where $$f_T \approx \frac{g_m}{2\pi C_{be}} \Rightarrow f_T \approx \frac{Y_{21}(v_{be})}{2\pi C_{be}} \text{ (Bipolar)} \quad (2)$$

$$f_T \approx \frac{g_m}{2\pi C_{gs}} \Rightarrow f_T \approx \frac{Y_{21}(v_{be})}{2\pi C_{gs}} \text{ (FET)} \quad (3)$$

From (1), R can be tuned by changing the bias-dependent $Y_{21}(v_{be})$ or by tuning the capacitor C_1 (or C_3) using varactors.

Since Y_{21} and C_{be} (if C_1 is embedded into the base-emitter or gate-source capacitance) are linked through the transistor transit frequency f_T, tuning of C_3 using varactor is effective way to synthesize ATR. However, tuning of C_3 using varactor diode affects the equivalent series capacitance value, resulting deviation in center frequency of the resonator.

Figure (3) shows the simplified model of 2-port ATR using small-signal device parameters of a MOSFET, including parasitic capacitance.

The characteristic of the 2-port ATR (R_{atr}) is given in terms of small signal [Y] parameters [5]

$$[Y] = \begin{bmatrix} \frac{1}{R_{atr}} + j\omega(C_P + C_{gd}) & -\left(g_m + \frac{1}{R_{atr}}\right) - j\omega C_P \\ -\frac{1}{R_{atr}} - j\omega C_P & \left(g_m + \frac{1}{R_{atr}}\right) + j\omega(C_P + C_{gs}) \end{bmatrix} \quad (4)$$

where $$R_{atr} = \frac{R_P \times R_{ds}}{R_P + R_{ds}} = \frac{R_P}{(1 + R_P \times g_{ds})} \Rightarrow g_{ds} = \left(\frac{1}{R_{atr}} - \frac{1}{R_P}\right) \quad (5)$$

From (4), $$R_{atr} = \frac{1}{\text{Re}[Y_{11}]}\bigg|_{\omega \to 0} \Rightarrow R_P = \frac{1}{\text{Re}[Y_{11}]}\bigg|_{\omega \to 0, V_{DS}=0} \quad (6)$$

$$(C_P + C_{gd}) = \frac{\text{Im}[Y_{11}]}{\omega}\bigg|_{\omega \to \infty} \quad (7)$$

$$g_{ds} = \left(\frac{1}{R_{atr}} - \frac{1}{R_P}\right)_{\omega \to 0} \quad (8)$$

$$V_{tune} \propto g_{ds} \Rightarrow V_{tune} \propto [R_{atr}]^{-1}, \quad V_{tune} \propto C_T \quad (9)$$

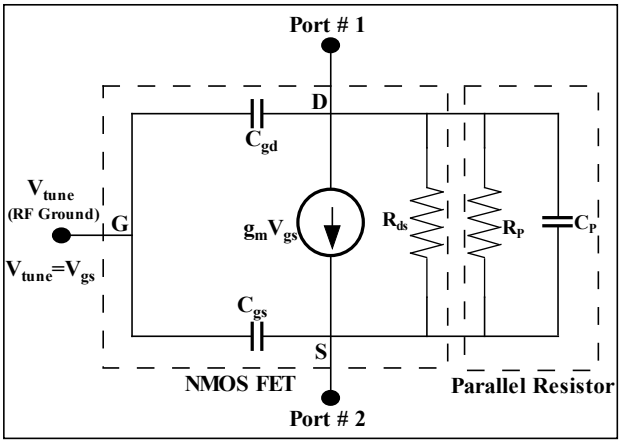

Fig.3. A typical representation of 2-port e model of ATR using MOSFET

From (9), R_{atr} can be tuned by varying V_{gs}, higher value of resistance exhibits lower parasitic capacitance, therefore, suited for reconfigurable oscillator at RF & MW frequencies.

B. Active Tunable Capacitor (ATC)

In general, tunable capacitors are characterized into four categories: (1) junction varactor, (2) MOS capacitor, (3) switched-capacitor array, and (4) MEMS based capacitors [5]. But their performances are limited by loss resistance and a package parasitic.

Figure (4) shows the typical schematic of active tunable capacitance (C_{atc}) using bipolar transistor.

The characteristics of capacitive feedback ATC can be described by (neglecting based-lead inductance, base-emitter capacitance and base-spreading resistance) (Fig. 5) [6]

$$C_{atc}(V_{be}) \approx \left[-\frac{Y_{21}(V_{be})}{\omega^2 C_1 C_2} + \frac{1}{j\omega \frac{C_1 C_2}{C_1 + C_2}} \right] \Rightarrow C_{atc}(V_{be}) = \left[-R(V_{be}) + \frac{1}{j\omega C_{in}(V_{be})} \right] \quad (10)$$

From (10), capacitance can be tuned by changing the bias dependent Y_{21} or by tuning the capacitor C_1 (C_{be}) or C_2 using varactors.

For practical implementation of the ATC, influences on the parasitic capacitances should be minimized.

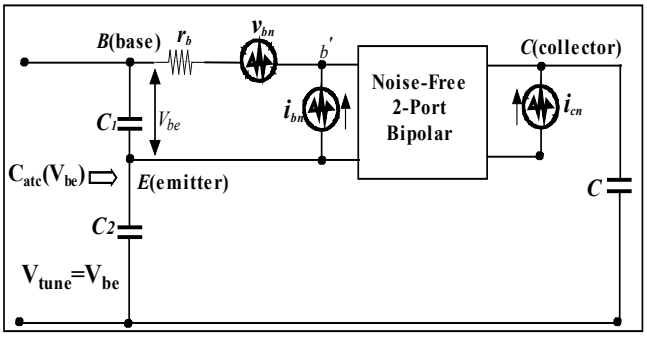

Fig.4. A typical equivalent representation of ATC using single transistor, including noise sources, which affects the dynamic ranges of ATC

C. *Active Tunable Inductor (ATI)*

The typical active inductor is based on gyrator, which can be realized by connecting inverting amplifier to non-inverting one in parallel and back-to-back. The electronic gyrator (Fig. 5) converts capacitor C into the inductance L, described by [8]

$$L(v) \approx \frac{C}{g_{m1} \times g_{m2}} \quad \text{(Ideal Case)} \qquad (11)$$

Figure (6) shows the complex impedance plot on Smith-chart that exhibits inductive behavior from 600MHz (#2) to 30 GHz (#5) but the real part of the input impedances are positive everywhere, therefore lossy and not a promising alternative.

Care must be taken to avoid encircling and crossing point 4.3 GHz (#3), which limits the applications. Grounded emitter cascode topology shows negative real part of the input impedance but gives band-limited operations (Fig.7) [9].

Figures (8) and (9) show the typical CAD simulated plot of equivalent inductance (imaginary part of Z_{22}) and resistance (real part of Z_{22}) at port 2 with respect to tuning voltage (Vt_{une}). It can be noticed that ATI circuit as shown in Figure (7), exhibits negative loss resistance region (Fig. 9) for $0.9V<V_{tune}<4.25V$, resulting high Q factor (> 500) tunable inductance.

Figures (10) and (11) show the typical schematic 12 GHz Colpitts oscillator circuit, plots of resonance frequency and phase noise using ATI described in Fig. (7).

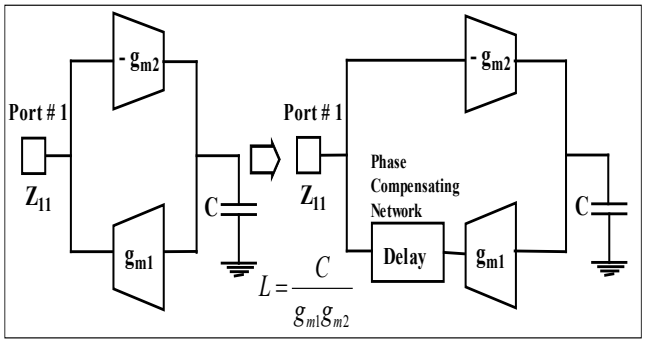

Fig.5. A typical equivalent representation of gyrator based active inductor

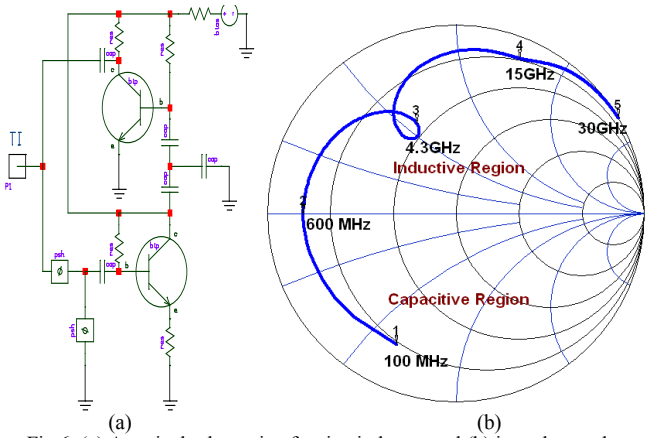

Fig.6. (a) A typical schematic of active inductor and (b) impedance plot

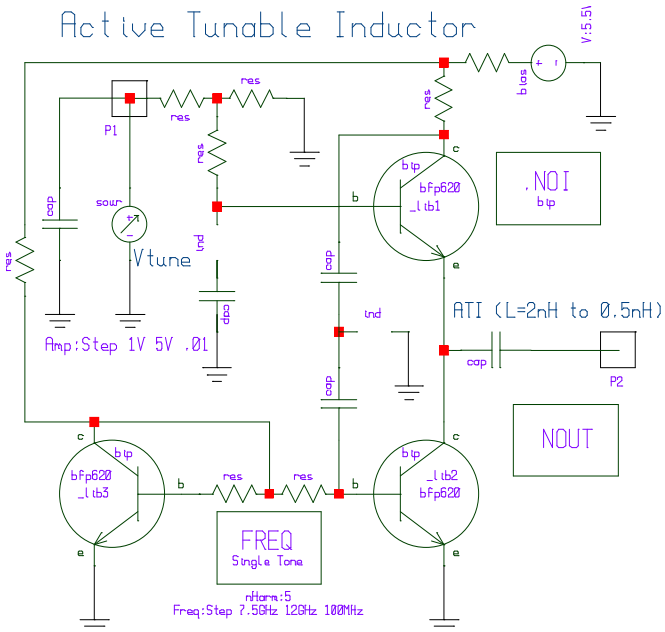

Fig. 7: A typical schematic of the ATI using bipolar (Infineon BFP 620)

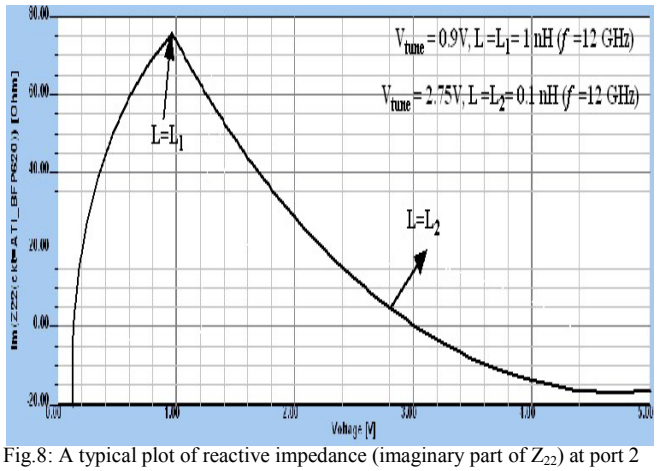

Fig.8: A typical plot of reactive impedance (imaginary part of Z_{22}) at port 2

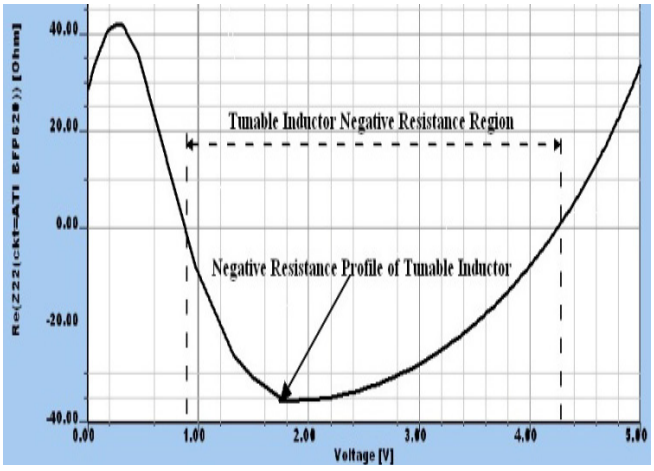

Fig.9: A typical plot of resistive impedance (real part of Z_{22}) at ATI port

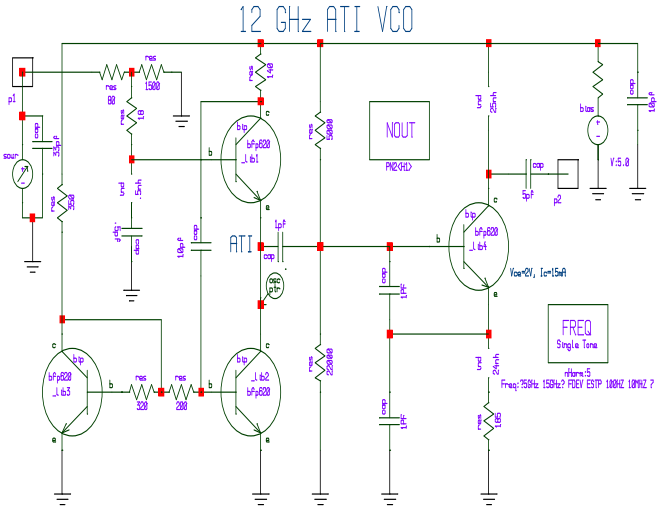

Fig. 10. A typical schematic of 12 GHz Colpitts oscillator using ATI circuit

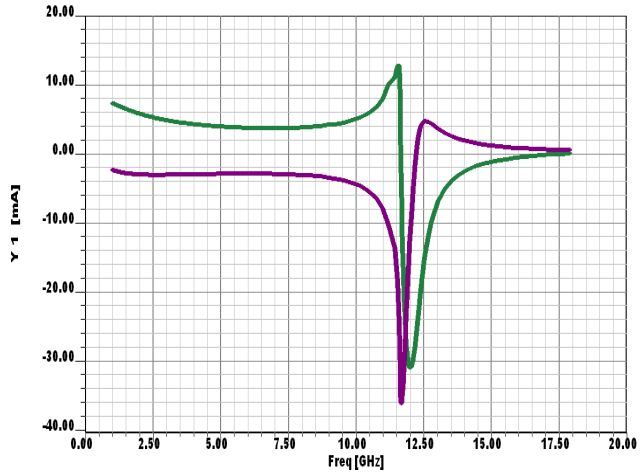

Fig.11: (a) Plots of resonance freq for the 12 GHz Colpitts oscillator (Fig. 10)

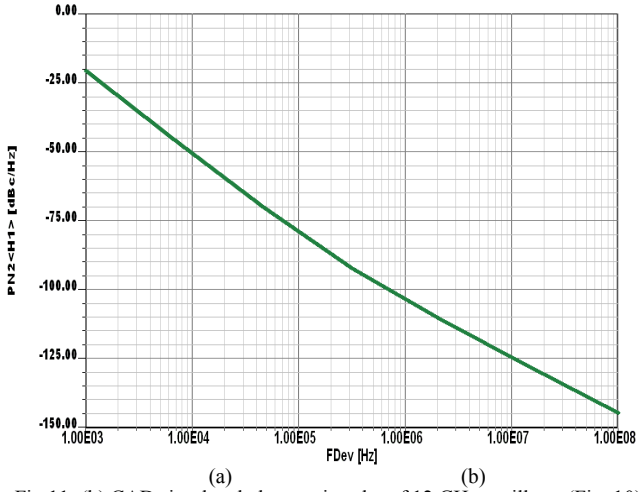

(a) (b)

Fig.11: (b) CAD simulated phase noise plot of 12 GHz oscillator (Fig. 10)

As shown in Figure (11), phase noise performance for 12 GHz ATI oscillator is inferior in comparison to commercially available varactor-tuned oscillators. Several approaches to overcome these problems have been considered, including the minimization of the noise introduced due to active devices which compose the ATI circuits. However, even these techniques result in power hungry and limited band characteristics because negative resistance generated in series with the inductance is not constant against the operating frequencies.

Figure (12) shows the typical schematic of power-efficient ATI, which is composed of common-source cascode FET's (FET1 and FET2) and a feedback FET (FET3).

As shown in Figure (12), the gate of FET3 is connected to the drain of FET1 and the source of FET2 for generating constant series negative resistance over the operating frequencies bands. The output impedance can be described by

$$Z_{out} = Z_{11} = R_{out} + \frac{j\omega C_{gs1}\left(\frac{1}{g_{m1}g_{m2}} + \frac{1}{g_{m1}g_{m3}}\right) - \frac{1}{g_{m2}}}{\left(1 - \frac{f}{f_T}\right)^2} \qquad (12)$$

By combining above described options, this paper reports the novel methodology for reconfigurable multi-band VCOs using ATR, which otherwise not possible with the varactor tuned VCOs for a given cost, size and power-consumptions.

The reported TAI VCO circuit using bipolar transistor (NEC 68830) compensates the losses incurred by ATR circuit by incorporating dynamic-mode drive-level (v_{be}) mechanism that optimizes the conduction angle and duty cycle for the minimum noise figure and also simultaneously generates dual frequency band with the user having an option of choosing a multiple distinct frequency or combination of them, eliminate the need of lossy switches for switching the frequency band, thereby improves the system throughput.

III. Reconfigurable VCOs

Frequency-band tuning, phase-noise tuning, and frequency-transconductance tuning can characterize the reconfigurability of the VCO.

Figure (13) shows the typical simplified schematic of multi-band ATI oscillator of n^{th} order that can be reconfigurable with respect to multi-band and multi-mode wireless systems.

For validation of this approach, dual-mode reconfigurable VCO is fabricated on a Rogers substrate with a dielectric constant of 3.38 and a thickness of 30mils (microstripline).

Figure (14) shows the typical dual-mode oscillation ω_1 or ω_2 or both ω_1 and ω_2. The measured phase noise as shown in Figure (15) for band #1 ((2.45-2.65 GHz) and band #2 (4.85-5.25GHz) are typically better than –118 dBc/Hz at 1MHz offset from the respective carrier frequencies. The circuit works on 3V, 20 mA and gives output power typically 3 dBm over the bands.

IV. Conclusion

With regard to the state of the art, dual-band ATI VCO reported in this work replaces varactor-tuned oscillators, and the technology is compatible with existing IC process.

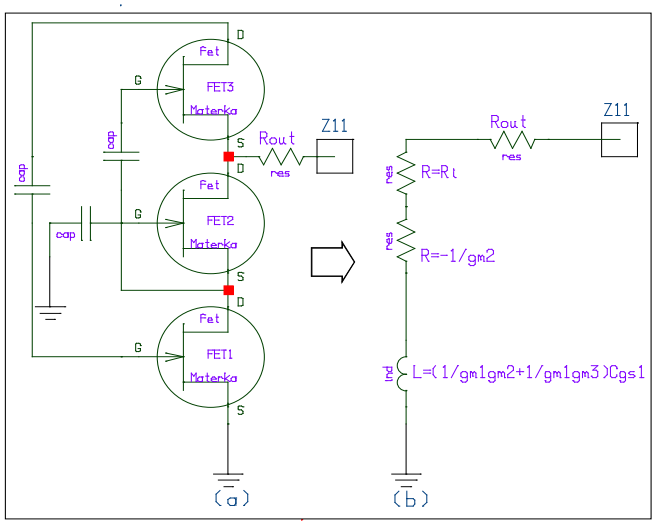

Fig.12. (a) A typical schematic of active inductor, (b) Simplified representation of circuit schematic shown in (a), considering FET equivalent circuit is assumed to be just a combination of the transconductance g_m and the gate-to-source capacitance C_{gs}, the output impedance Z_{11}

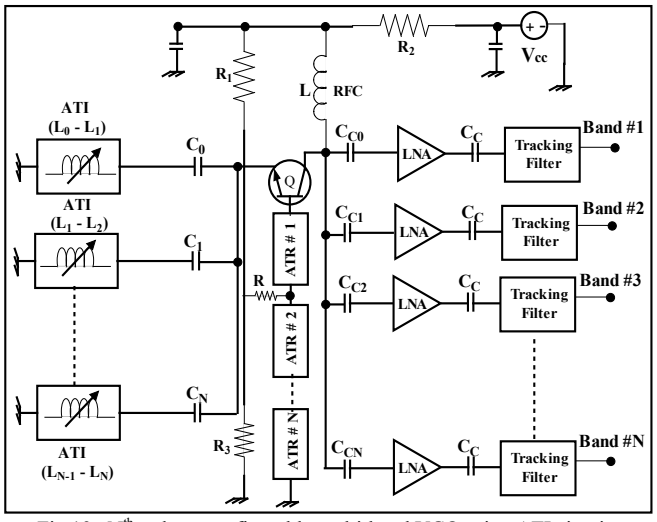

Fig.13. N^{th} order reconfigurable multi-band VCO using ATI circuits

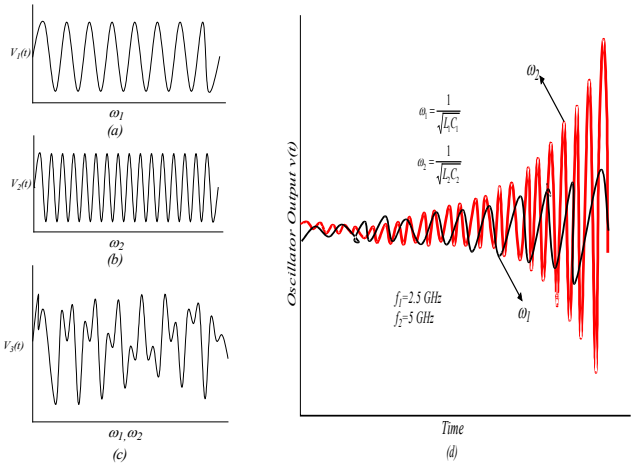

Fig. 14. (a) Steady state oscillations at ω_1, (b) Steady state oscillations at ω_2, (c) Simultaneous oscillations at ω_1 and ω_2 (d) Growth of oscillations

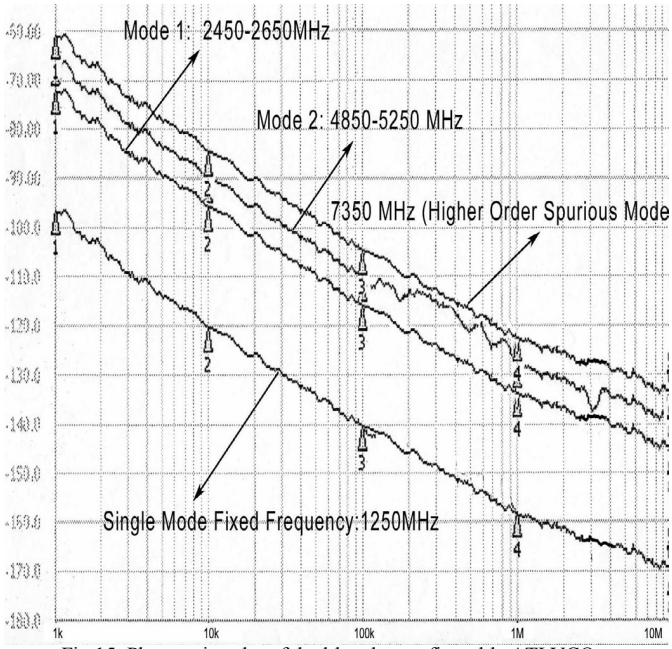

Fig.15. Phase noise plot of dual-band reconfigurable ATI VCO

REFERENCES

[1] U. L. Rohde and A. K. Poddar, "Reconfigurable Concurrent Voltage Controlled Oscillator (RVCO), IEEE/APMC 2007, pp. Dec. 11-14, 2007, Bangkok, Thailand.

[2] J Ryynanen, S. Lindfors, K. Stadius, and K. Halonen, :Integrated Circuits for Multi-Band Multi-Mode Receivers", IEEE Circuits and System Magazine, second quarter 2006, pp.5-15.

[3] H. L. Kao, D. Y. Yang, A. Chin, and S. P. McAlister, "A 2.4/5GHz Dual-Band VCO using a Variable Inductor and Switched Resonator," 2007 IEEE-MTT-S, Digest, pp. 1533-1536.

[4] R. Kaunisto, " Monlithic Active Resonator Filters For High Frequencies", Dr. of Science in Tech. Dissertation, H. U. of Technology, Finland, Nobember 2000.

[5] R. Mukhopadhyay, Y. Park, P. Sen, N. Srirattana, J. Lee, C-H Lee, S. Nuttinck, A. Joseps, J. D. Cressler, and J. Laskar, " Reconfigurable RFICs in Si-Based Technologies for a Compact Intelligent RF Front-End", IEEE Trans. On MTTT, Vol. 53, No.1, pp. 81-93, Jan 2005.

[6] U. L. Rohde, A. K. Poddar, and G. Boeck, Modern Microwave Oscillators for Wireless Applications: Theory and Optimization, Wiley, NY, 2005.

[7] S. Hara et al., " Lossless broadband monolithic microwave active inductors," IEEE Trans. On MTT, vol.37, no. 12, pp. 1979-1984, Dec. 1989.

[8] S. Del Re, G. Leuzzi and V. Stornelli, "A New Approach to the Design of High Dynamic Range Tunable Active Inductors", Integrated Nonlinear Microwave and Millimeter-Wave Circuits, 2008, pp. 25-28, INMMIC 2008

[9] E. Sonmez, P. Abele, K.-B. Schad and H. Schumacher, "16 GHz Integrated Oscillator Design with Active Elements in a Production Ready SiGe HBT MMIC Technology," EUMC, Paris, France, October 02-06, 2000.

[10] P. Alinikula, et al., " Monlithic active resonators for wireless applications," IEEE MWWMC Symposium, pp. 197-199, 1994/

[11] V. Pauker, " GaAs monloithic microwave active gyrator, " IEEE GaAa IC Symp., pp. 82-84, 1986.

[12] S. Lucyszn, et al., Monolithic narrowband filter using ultra Q tunable active inductors," IEEE Trans. On MTT, Vol. 42, no. 12, pp. 2617-2622, Dec 1994.

[13] K. W. Kobayashi, et al., “A novel heterojunction bipolar transistor VCO using an active tunable inductance,” IEEE Microwave and Guided Wave Lett., vol. 4, no. 7, pp. 235-237, Jul 1994.

[14] Jin-Su-Ko and K. Lee, “ Low power, tunable active inductor and its applications to monolithic VCO and BFP,” 1997 IEEE MTT-S, pp. 929-932.

[15] H. Hayashi, M. Muraguchi, Y. Umeda, and T. Enoki, “A High-Q Broad-Band Active Inductor and Its Application to a Low-Loss Analog Phase Shifter”, IEEE Trans. On MTT, Vol. 44, No. 12, Dec 1996.